NeuroImage 227 (2021) 117628

Contents lists available at ScienceDirect

NeuroImage

journal homepage: www.elsevier.com/locate/neuroimage

Spatiotemporal functional interactivity among large-scale brain networks

Nan Xu [a,*], Peter C. Doerschuk [b,c], Shella D. Keilholz [a], R. Nathan Spreng [d,e,f,g]

[a] Wallace H. Coulter Department of Biomedical Engineering, Georgia Institute of Technology and Emory University, Atlanta, GA, United States
[b] School of Electrical and Computer Engineering, Cornell University, Ithaca, NY, United States
[c] Nancy E. and Peter C. Meinig School of Biomedical Engineering, Cornell University, Ithaca, NY, United States
[d] Laboratory of Brain and Cognition, Department of Neurology and Neurosurgery, Montreal Neurological Institute, McGill University, Montreal, QC, Canada
[e] Departments of Psychiatry and Psychology, McGill University, Montreal, QC, Canada
[f] Douglas Hospital Research Centre, Montreal, QC, Canada
[g] McConnell Brain Imaging Centre, Montreal Neurological Institute, McGill University, Montreal, QC, Canada

ARTICLE INFO

Keywords:
Spatiotemporal functional interactivity
Directed functional connectivity
Information flow
Functional networks
Resting-state fMRI

ABSTRACT

The macro-scale intrinsic functional network architecture of the human brain has been well characterized. Early studies revealed robust and enduring patterns of static connectivity, while more recent work has begun to explore the temporal dynamics of these large-scale brain networks. Little work to date has investigated directed connectivity within and between these networks, or the temporal patterns of afferent (input) and efferent (output) connections between network nodes. Leveraging a novel analytic approach, prediction correlation, we investigated the causal interactions within and between large-scale networks of the brain using resting state fMRI. This technique allows us to characterize information transfer between brain regions in both the spatial (direction) and temporal (duration) scales. Using data from the Human Connectome Project (N = 200) we applied prediction correlation techniques to four resting-state fMRI scans (each scan has TRs = 1200). Three central observations emerged. First, the strongest and longest duration connections were observed within the somatomotor, visual, and dorsal attention networks. Second, the short duration connections were observed for high-degree nodes in the visual and default networks, as well as in the hippocampus. Specifically, the connectivity profile of the highest-degree nodes was dominated by efferent connections to multiple cortical areas. Moderate high-degree nodes, particularly in hippocampal regions, showed an afferent connectivity profile. Finally, multimodal association nodes in lateral prefrontal brain regions demonstrated a short duration, bidirectional connectivity profile, consistent with this region's role in integrative and modulatory processing. These results provide novel insights into the spatiotemporal dynamics of human brain function.

1. Introduction

Human brain function at rest (i.e. in the absence of task) is characterized by coherent and persistent patterns of regional interactions organized into spatially distributed, large-scale networks (Cole et al., 2014). These intrinsic patterns emerge from repeated co-activation of afferent (input) and efferent (output) connections among brain regions (Stevens and Spreng, 2014). Resting-state functional magnetic resonance imaging (fMRI), which examines the low-frequency spontaneous fluctuations in blood oxygen level dependent (BOLD) signals (Biswal et al., 1995), is widely used to investigate the intrinsic functional architecture of the brain. Substantial progress has been made in delineating large-scale functional brain networks using resting-state functional connectivity (RSFC) (e.g., Biswal et al., 1995; Power et al., 2011; Yeo et al., 2011). The most commonly used method for measuring RSFC is to calculate a pairwise correlation coefficient between the low-frequency BOLD signals of a set of priori determined brain regions of interest (ROIs). These correlation matrices may then be used to model the spatial topology of functional networks and sub-networks (Sporns, 2011; Wig et al., 2011).

In the last decade, substantial efforts have been devoted to identifying the spatiotemporal structure of these RSFC-derived brain networks. However, comparatively less effort has been focused on identifying directional or 'effective' connectivity patterns. Several computational approaches have been suggested to explore directed intrinsic connectivity (e.g., Blinowska et al., 2009; Chen et al., 2011; Kim et al., 2007; Roebroeck et al., 2005; Xu et al., 2017). In parallel, several studies have revealed that correlated, yet temporally asynchronous, patterns of BOLD

* Corresponding author.
E-mail addresses: im.nan.xu@gmail.com (N. Xu), pd83@cornell.edu (P.C. Doerschuk), shella.keilholz@bme.gatech.edu (S.D. Keilholz), nathan.spreng@gmail.com (R.N. Spreng).

https://doi.org/10.1016/j.neuroimage.2020.117628
Received 2 September 2020; Received in revised form 21 November 2020; Accepted 3 December 2020
Available online 13 December 2020

signals may reflect the timing of information transfer in the brain (e.g., Goelman et al., 2017; Mitra et al., 2015; Xu et al., 2017; Yuste and Fairhall, 2015). Together, these advances open the possibility of identifying not only the spatial properties of these intrinsic brain networks but also the direction and rate of information flow through this network architecture.

We have developed a novel statistical approach, prediction correlation (p-correlation, Xu et al., 2017) to measure the direction and temporal profile of intrinsic functional connections. P-correlation provides a single analytical technique to characterize the strength, direction, and timing of connections simultaneously. We have validated the p-correlation approach using synthetic data for direction estimation and resting-state fMRI (rs-fMRI) data to estimate connection strength (Xu et al., 2017). Specifically, testing on the simulated fMRI timeseries from the laboratory of S.M Smith (Smith et al., 2011) which are available on-line (http://www.fmrib.ox.ac.uk/analysis/netsim/), the performance of p-correlation was numerically compared with and has outperformed a list of alternative effective connectivity estimation methods, including Granger causality, against the ground truth. In addition, testing on the experimental data from the 1000 Functional Connectomes Project (http://www.nitrc.org/projects/fcon_1000/) (Biswal et al., 2010), the capability of p-correlation in recovering the previously identified network organization of the human brain by the standard correlation was demonstrated. As p-correlation decomposes asynchronous pairwise functional interactivity, we are able to derive 'direction' as well as 'duration' information to characterize node to node connectivity profiles within and between networks. This approach is in contrast to symmetric estimates of RSFC as measured by standard Pearson correlation methods. To distinguish these measures from standard pairwise, symmetric *functional connectivity* (FC) measured by Pearson correlation, we refer to the functional interactivity measured by p-correlation as *directed functional connectivity* (directed FC) and *directed RSFC* for intrinsic network measures obtained at rest.

In the current study, we apply p-correlation to rs-fMRI data to investigate the directed intrinsic functional connectivity of the human brain. To characterize the temporal flow of information through the networks, we first identified the duration (long versus short) of asynchronous connections across the brain and their spatial overlap with known intrinsic brain networks. Next, we examined the asymmetry of the pairwise spatiotemporal functional interactivity. Our reasoning here was that p-correlation decomposes the pairwise functional interactivity to inward and outward information transfers, providing directional estimations. To our best knowledge, this is the first work in which the brain-wide spatial and temporal patterns of pairwise functional interactivities are jointly examined.

2. Methods

2.1. Participants and data preprocessing

The rs-fMRI data of 200 randomly-selected unrelated individuals were downloaded from the Human Connectome Project 500 Subjects + MEG2 dataset (https://www.humanconnectome.org/study/hcp-young-adult/document/500-subjects-data-release) (Marcus et al., 2011; Van Essen et al., 2012). This cohort of 200 participants was aged 22–36 years (mean age= 28.9 ± 3.5 years), with 126 women.

The rs-fMRI data were collected at Washington University in St Louis and the University of Minnesota with the same sampling rate, $TR = 0.72$s. Each subject has 4 complete rs-fMRI scans, and each scan has 1200 time samples, i.e., $N_x = 1200$. Other acquisition parameters include TE=33.1 ms, flip angle=52°, FOV=208 × 180 mm (RO x PE), Matrix 104 × 90 (RO x PE), Slice thickness=2.0 mm with 72 slices and 2.0 mm isotropic voxels, Multiband factor=8, Echo spacing=0.58 ms, and BW=2290 Hz/Px.

The rs-fMRI data were first preprocessed following the procedures detailed in (Glasser et al., 2013) to remove spatial distortions, motion artifacts, and reduce field bias. This procedure also registered the functional and anatomical images and normalized the data to standard space. The output fMRI data was then denoised by the ICA-FIX approach as described in detail in (Griffanti et al., 2014; Salimi-Khorshidi et al., 2014). Finally, the preprocessed rs-fMRI BOLD timeseries were extracted from 333 ROIs (N_{ROI}=333). These were centered in 333 discrete brain parcels provided in Gordon et al. (2016). In the remainder of the paper, we refer the resulting dataset as the extracted rs-fMRI timeseries.

In addition to the extracted rs-fMRI timeseries, shuffled data and phase randomized data were also generated. The generation procedures and results are detailed in the Supplementary Methods and Results. The purpose of data shuffling or randomizing the phase of the data is to randomize the spatiotemporal dynamics of the original rs-fMRI timeseries. These results can then be used to contrast the spatiotemporal structure estimated from the original data to validate the analytical approach under testing.

2.2. Mathematical description of the spatiotemporal functional interactivity

The spatiotemporal functional brain activity may be decomposed into two components, 1) the spatially directed FC and 2) the temporal durations of information transfer of this directed FC. In this section, we briefly review the mechanism of prediction correlation (p-correlation) introduced in Xu et al. (2017) and describe how these two patterns are estimated from p-correlation.

Let x_i and x_j be the BOLD signals of N_x samples which come from the ith ROI and the jth ROI, respectively. P-correlation of the ordered pair (x_i, x_j) involves several computational steps. The first step estimates the duration of information transfer from the ith ROI and the jth ROI. Specifically, the output signal x_j is predicted from the input signal x_i through a linear time-invariant causal dynamic model that characterizes the information transfer, and the prediction, denoted by $x_{j|i}$, has the form

$$x_{j|i}[n] = \sum_{m=0}^{N_{j|i}-1} h_{j|i}[m] x_i[n-m], \tag{1}$$

$$\text{and } x_j[n] = x_{j|i}[n] + \varepsilon[n], \tag{2}$$

where $h_{j|i}$ is a $N_{j|i}$-length impulse response vector which has the first potentially non-zero term occurred at time of 0 s, and ε is the prediction error. The current sample of the output signal x_j is always effected by $N_{j|i}$ time lags of the input signal x_i. Hence, the duration of the directed information transfer has $TR \cdot N_{j|i}$ seconds. The optimal solution for $N_{j|i}$ is determined by Bayesian information criterion (BIC) through testing from 1 up to $\frac{D}{TR}$ samples to minimize the prediction error. In this study, we restrict the temporal window for directional influence between ROIs to be no more than 15 s, i.e., D =15 s.

The second step estimates the strength of the RSFC between the ordered pair (x_i, x_j), denoted by p-corr(x_i, x_j). Specifically, a correlation between the predicted signal $x_{j|i}$ and the original BOLD signal x_j is computed.

$$\text{p-corr}(x_i, x_j) = \text{corr}(x_{j|i}, x_j), \tag{3}$$

Note that if the signal x_j and its prediction $x_{j|i}$ are significantly correlated, i.e., the result of Eq. (3) is high, then the likelihood of a directed information transfer as modeled in Eqs. (1)–(2) is high. The significance of the p-correlation can be determined by a p-value test. The p-value at which the null hypothesis of zero p-correlation is rejected (probability whose small value indicates a significant p-correlation) can be computed by following the procedure in Press et al. (2007).

As described in Xu et al. (2017), p-correlation is able to replicate previously observed modular network structures in the resting brain (Power et al., 2011). Thus, p-corr(x_i, x_j) can be used to evaluate the strength of RSFC from ith ROI to the jth ROI. However, unlike the standard correlation, p-correlation is asymmetric between the two signals x_i

and x_j. Specifically, p-corr(x_i, x_j) ≠ p-corr(x_j, x_i) and $N_{j|i} \neq N_{i|j}$. The asymmetry between p-corr(x_i, x_j) and p-corr(x_j, x_i) leads to a directed graph between two brain regions in the spatial scale. In addition, the separate estimations for $N_{i|j}$ and $N_{j|i}$ characterizes the interactions in the temporal scale.

For the whole-brain fMRI timeseries, two $N_{ROI} \times N_{ROI}$ asymmetric matrices were generated by p-correlations. One is a connectivity matrix including p-correlation values (e.g., p-corr(x_i, x_j) from Eq. (3)). The other is a duration matrix including the duration of the information transfer (e.g., $TR \cdot N_{j|i}$) estimated from Eq. (1–2).

2.3. Analytical procedures

In this section, the analytical procedures for investigating the spatiotemporal structure estimated from p-correlation are described. First, the spatial pattern and the temporal pattern of the functional interactivity were determined by p-correlation using the extracted rs-fMRI timeseries. Specifically, a directed FC matrix and a duration matrix was determined by averaging the connectivity matrices and the duration matrices across all scans of all 200 subjects, respectively. To validate the spatiotemporal patterns estimated by p-correlation on the extracted rs-fMRI timeseries, the directed FC matrix and duration matrix were contrasted with the results of the shuffled data and the results of the phase-randomized data (see Supplementary Methods and Results for more details). Seven functional networks provided in Yeo et al. (2011) were used in the remainder analysis, which include Somatomotor (SM), Visual, Dorsal, Ventral, Default, Frontal parietal (FP), and Limbic networks (see Supplementary Methods and Results for more details).

Next, we investigated the dominant network properties driven by directed RSFC with the long and short duration of information transfer in the human brain. In particular, the long durations of information transfers determined by the top 4% values in the duration matrix were compared with the strongest connections as determined by the top 4% values in the functional matrix. The threshold of the top 4% was selected because the community detection algorithm Infomap can roughly detect the 7 distinct Yeo networks drawing from the top 4% of the directed FC matrix estimated by p-correlation as is described in the Supplementary Methods and Results. A similar finding was discovered by using the same algorithm on p-correlation or correlation matrix computed from a different dataset in the 1000 Functional Connectomes Project (Fig. 8 (Xu et al., 2017)). Specifically, major distinct Power communities (Power et al., 2011) were detected at the threshold of 4% (see Fig. 8 in (Xu et al., 2017)). The directed RSFC with the short durations of information transfer were determined by the smallest 4% nonzero values in the duration matrix which has p-value<0.05 in the directed FC matrix. To ensure the robustness of the results, the same analysis was performed on two split cohorts from the 200 participants, each cohort with 100 participants, and the results are shown in Section 3 of Supplementary Methods and Results.

The functional interactivity among networks was evaluated for the directed FC matrix as well as the duration matrix, and is described in the Supplementary Methods and Results. During the analysis of the directed RSFC with short durations, we observed that the short duration connections are driven by “hub” that either aggregates the incoming information from (inward) or propagates information to (outward) the rest brain cortex (as is described below in Section 3.2). We computed the degree of each ROI, which is the total number of edges that converge on that ROI (Buckner et al., 2009; see also Power et al., 2013). Specifically, given the directed short duration matrix determined above, the degree of each “inward ROI” is the total number of nonzero entries in each matrix column, whereas the degree of each “outward ROI” is the total number of nonzero entries in each matrix row.

Then, we assessed the asymmetry between the inward and outward information transfer for each ROI. In particular, the following five steps were performed. First, a matrix containing the standardized z-scores of the pairwise directed FC was computed, namely the directed FC z-score matrix. Similarly, a directed duration z-score matrix was computed. Second, the lower off-diagonal entries were subtracted from their upper off-diagonal counterparts (referred to as the afferent-efferent, or inward-outward differences in the remainder of the paper) in both the directed FC z-score matrix and duration z-score matrix. Third, the sample mean and standard deviation of the inward-outward differences were computed, denoted by (μ_{FC}, std_{FC}) for the directed FC inward-outward differences and (μ_D, std_D) for the directed duration inward-outward differences. In addition, the correlation between the upper and lower triangular entries was computed for each of the two z-score matrices. Fourth, to test if the inward-outward differences are significantly different from a mean of zero, a one-sample hypothesis test was set up on the sample mean of inward-outward differences for directed FC as well as for the directed duration, respectively. Specifically, for the directed durations case, the null hypothesis $H_0 : \mu_D = 0$ was tested against the alternative $H_1 : \mu_D \neq 0$. The same hypothesis test was set up for the directed FC case (e.g., $H_0 : \mu_{FC} = 0$ versus $H_1 : \mu_{FC} \neq 0$). Because the sample size for these two sample distributions of inward-outward differences are both $N_{sample} = (N_{ROI}^2 - N_{ROI})/2 = 55,278$, the central limit theorem holds, implying that the two distributions are approximately normal (p.228-p229 Montgomery and Runger, 2010)). Therefore, a z-test was formed for each of these two hypothesis tests with the test statistics $Z_{FC0} = \frac{\sqrt{N_{sample}}\mu_{FC}}{std_{FC}}$ for the directed FC strength case and the test statistics $Z_{D0} = \frac{\sqrt{N_{sample}}\mu_D}{std_D}$ for the directed duration case. The two z-tests were separately evaluated at a significance level of $\alpha = 5\%$ following the test procedure as described in p.302 (Montgomery and Runger, 2010). Fifth, we tested which inward-outward differences sample between the directed FC and duration has a mean closer to zero (e.g., $\mu_0 = 0$). Specifically, a two-sample hypothesis test was set up with the null hypothesis $H_0 : |\mu_D - \mu_0| = |\mu_{FC} - \mu_0|$ and the alternative $H_1 : |\mu_D - \mu_0| > |\mu_{FC} - \mu_0|$. Because both μ_{FC} and μ_D turned out to be negative in the third step calculation, the proposed two-sample hypothesis test becomes equivalent to a two-sample z-test with $H_0 : \mu_D = \mu_{FC}$ and $H_1 : \mu_D < \mu_{FC}$, and the test statistics $Z_0 = \frac{\sqrt{N_{sample}}(\mu_D - \mu_{FC})}{\sqrt{std_D^2 + std_{FC}^2}}$. Following the procedure described in p.355, Eq. (10-(2) (Montgomery and Runger, 2010), this two-sample z-test was evaluated at a significance level of $\alpha = 5\%$. To demonstrate the robustness of the test results concerning the inward-outward differences, the five-step procedure was also performed on two split cohorts from the 200 participants, each cohort with 100 participants, and the results are shown in Section 6 of Supplementary Methods and Results.

Finally, due to the novelty of the directed duration matrix estimation, its inward and outward asymmetries were examined in more detail. Specifically, for each of the 333 ROIs, the row mean and the column mean of the duration matrix were computed to give the average durations of the inward and outward information transfers, respectively. Furthermore, the duration matrix was partitioned into 7×7 subblocks, in which the diagonal subblocks include the connectivity within functional networks and the off-diagonal subblocks include the connectivity between different pairs of networks. The average duration of the inward (outward) information transfer for the ith functional brain network was determined by computing the mean and standard deviation of entries in the ith column (row) partition excluding the ith diagonal subblock of the duration matrix, for $i = 1, \ldots, 7$.

3. Results

3.1. Long duration rs-fMRI network connectivity

The directed FC matrix and the duration matrix estimated from p-correlation is shown in Fig. 1(a) and Fig. 1(b), respectively. Note that global signal regression was not applied to rs-fMRI data in the current study due to the current controversial effects (Murphy and Fox, 2017). Hence, p-correlation values are mostly positive in Fig. 1(a). As shown,

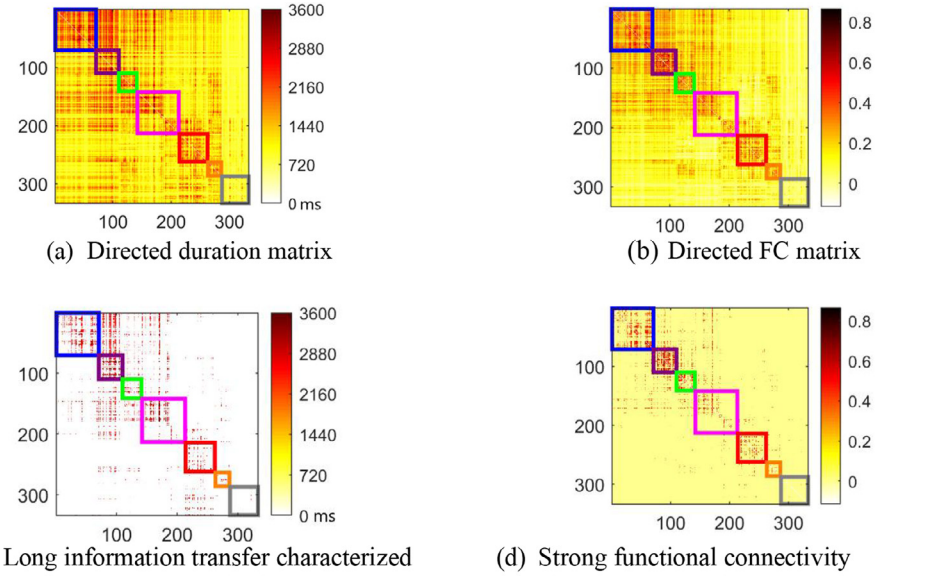

(a) Directed duration matrix

(b) Directed FC matrix

(c) Long information transfer characterized by the top 4% values in the duration matrix in (a)

(d) Strong functional connectivity characterized by the top 4% values in directed FC matrix in (b)

Fig. 1. The directed duration matrix and the directed functional connectivity matrix of resting-state functional networks determined by p-correlations. In these asymmetrical matrices, ROIs along the rows propagate information to the ROIs along the columns. The strongest directed FC and the longest information transfers are shown in (c) and (d), respectively. Seven colored diagonal blocks in each matrix depict the seven different networks including SM (blue), Visual (purple), Dorsal (green), Ventral (pink), Default (red), FP (orange), Limbic (gray).

organized patterns are demonstrated in both the directed FC and duration matrices. In particular, the strong connections are concentrated in the diagonal blocks, suggesting that connections within each functional network on average are stronger than the ones between this network and the other networks. Similar to the directed FC matrix, the high values of the duration matrix are also concentrated within the diagonal blocks, with high overlap between strong and long duration functional connections. The correlation between the directed FC matrix and the duration matrix was computed for each scan of each subject. The averaged correlation value turns out to be 0.64 ± 0.06 across 4 scans and 200 subjects for the extracted rs-fMRI timeseries. As a comparison, the correlation between the two matrices was also computed for each scan of the five phase-randomized subjects (see Supplemental Methods and Results Table S1). As a result, the averaged correlation across 4 scans and five subjects is, however, only 0.27 ± 0.03, in contrast to the averaged correlation value without randomizing the phase which is 0.65 ± 0.05.

The top 4% of values in either of these two matrices are further shown in Fig. 1(c) and (d), respectively. The strongest directed connections and the longest durations occur primarily within-networks, including the SM, visual and ventral systems. Longer durations were also observed between networks (e.g. SM - Visual networks). On the other hand, directed functional interactivities within the limbic system have much lower values in both matrices comparing to other functional networks. This may be due to the low temporal SNR of the fMRI timeseries of the limbic ROIs. Similar results were reported in Fig. S1 (Power et al., 2011) using 1000 Functional Connectomes Project (http://www.nitrc.org/projects/fcon_1000/) (Biswal et al., 2010).

3.2. Short-duration rs-fMRI network connectivity

The duration matrix and the corresponding directed RSFC matrix with short information transfers as described in Section 2.3 are shown in Fig. 2(a) and (b), respectively. In each of these two matrices, nonzero entries demonstrate the duration or strength of the directed RSFC with short information transfer. The directed RSFC is further rendered on the brain cortex in Fig. 2(c). The smallest 4% nonzero values in the duration matrix (without considering the p-value for p-correlations) and the corresponding connectivity matrix are shown in Figure S8 of Supplementary Methods and Results. In Fig. 2(a) and (b), the directed RSFC with short information transfer has an average duration of 743.19 ms $\pm$ 10.04 ms, and has an average strength of 0.10 $\pm$ 0.04. While the variability of both functional strengths and duration is low in these two matrices, a "hub-like" structure appears to be the dominant feature among these connections. We discuss this in the next paragraph.

High degree ROIs are those with extensive functional connections relative to other brain networks. These may serve as information processing hubs (Buckner et al., 2009; see also Power et al., 2013). As observed in Fig. 2, the short duration connections are dominated by sparse rows and columns with widespread connections throughout the brain, in contrast to the long duration connections that are dominated by denser and modular connections as shown in Fig. 1(c). These sparse rows and columns represent high degree ROIs. Further, rows with dense dotted lines of the two matrices shown in Fig. 2 suggest that these high degree, short duration hubs primarily are dominated by efferent connections to other ROIs and networks, and we name them as "outward brain hubs." However, the columns with less dense dotted lines in the two matrices in Fig. 2 also identify short duration, high degree hubs that show a predominantly afferent, or inward, connectivity pattern, and these hubs were named "inward brain hubs."

High-degree outward and inward brain hubs are displayed on cortical maps in Fig. 3(a) and (b), respectively. Efferent or outward brain hubs with the highest degree are located in the visual system and the default system, in particular, the angular gyrus. Specifically, the top 5 outward brain hubs (Fig. 3(a)) are #263 in Visual (degree 181), #259 in Default (degree 121), #140 in Visual (degree 110), #94 in Default (degree 88), #6 in Default (degree 63).[1] Afferent (or inward) brain hubs with high degrees are primarily located in the limbic system. The top 14 inward brain hubs (Fig. 3(b)) include #178 in Limbic (degree 31), #19 in Limbic (degree 27), #135 in Limbic (degree 21), #18 in Limbic (degree 18), #11 in Limbic (degree 18), #314 in Limbic (degree 17), #144 in Limbic (degree 17), #300 in Limbic (degree 15), #118 in Limbic (degree 15), #312 in Limbic (degree 14), #142 in Limbic (degree 14), #304 in Limbic (degree 13), #296 in Limbic (degree 13), and #295 in Default (degree 13).[1] Both afferent and efferent hubs show high hemispheric symmetry. The efferent hubs have higher degree values than the hubs that demonstrate a more afferent, or inward, pattern of directed connectivity. To demonstrate the robustness of the results, the top in-

[1] The # is consistent with the order of the 333 ROIs provided in Gordon et al. (2016).

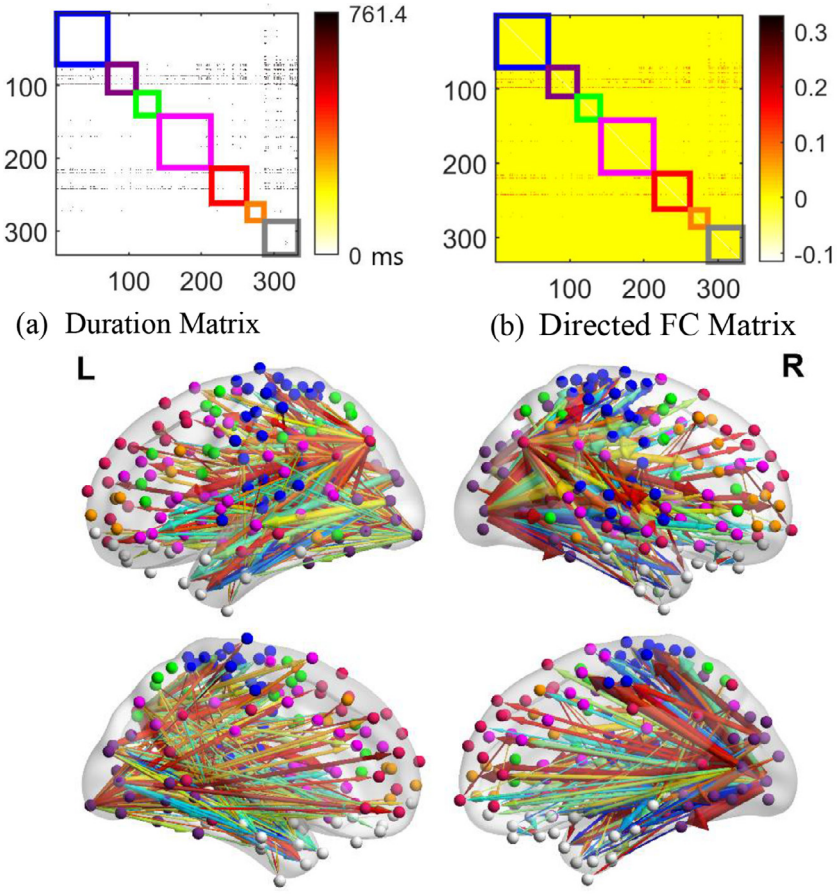

Fig. 2. Short information transfer, characterized by the shortest 4% nonzero $N_{j|i}$ values and p-correlations with p-value<0.05. The duration matrix (a) and the directed functional connectivity matrix (b) of the short information transfer in rs-fMRI. In both matrices, ROIs along the rows propagate information to the ROIs along the columns. Seven colored diagonal blocks in (a) and (b) depict the seven different networks as described in the legend (right). (c) The brain regions and the directed functional connections with the shortest information transfer are displayed on the brain cortex. The color of the arrow from cool to warm colors represents the duration from long to short. The thickness of the arrow represents the strength of the connectivity. In total, 1001 directed functional connections are demonstrated. Seven colored diagonal blocks in (a) and (b) as well as the node color in (c) depict the seven different networks including SM (blue), Visual (purple), Dorsal (green), Ventral (pink), Default (red), FP (orange), Limbic (gray). A modified version of BrainNet Viewer toolbox (Xia et al., 2013) was used.

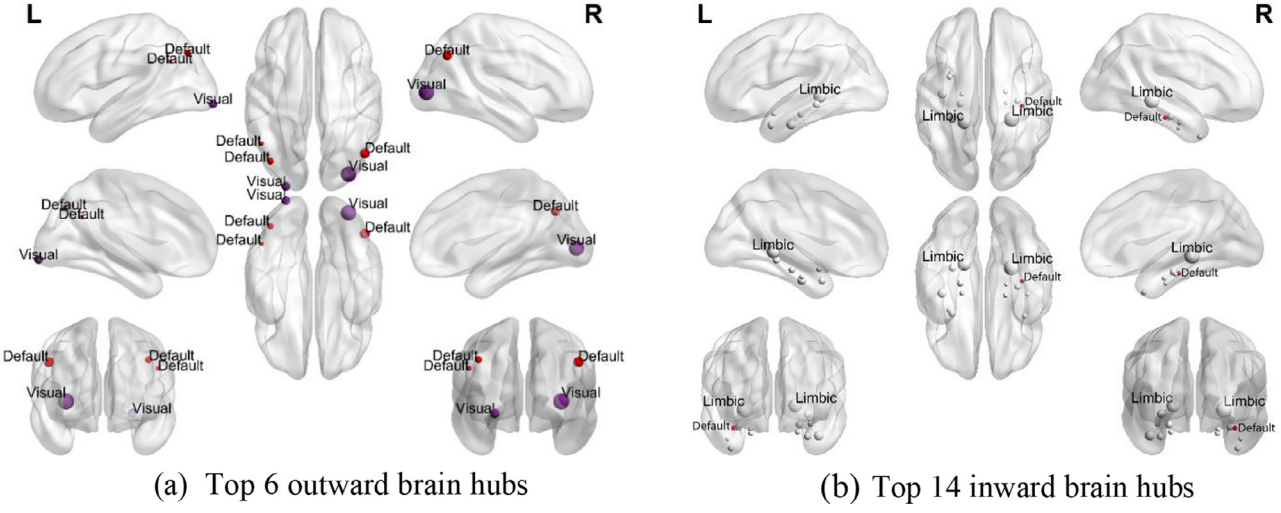

Fig. 3. Brain hubs displaying short information transfer in function networks. The node color represents the brain system of visual (purple), default (red), and limbic (white). The node size is proportional to the hub degree in each subfigure.

ward and outward hubs were also plotted for each of the two randomly split cohorts in Section 3 of the Supplementary Methods and Results.

3.3. Asymmetries between the inward and outward information transfer

Asymmetries between inward and outward information transfer exist in both the directed FC matrix and duration matrix for every pair of ROIs (Fig. 1) as well as for every pair of functional networks (Fig. S2). To visualize the asymmetries in detail, the information of the connectivity strength (Fig. 1(a)) and duration (Fig. 1(b) matrices are shown in Fig. 4. This figure displays the top 25 strongest directed connections within, going out of, and coming into each of the seven functional brain networks. The top 50, 75, and 100 strongest directed connections within, going out of, and coming into each of the seven functional brain net-

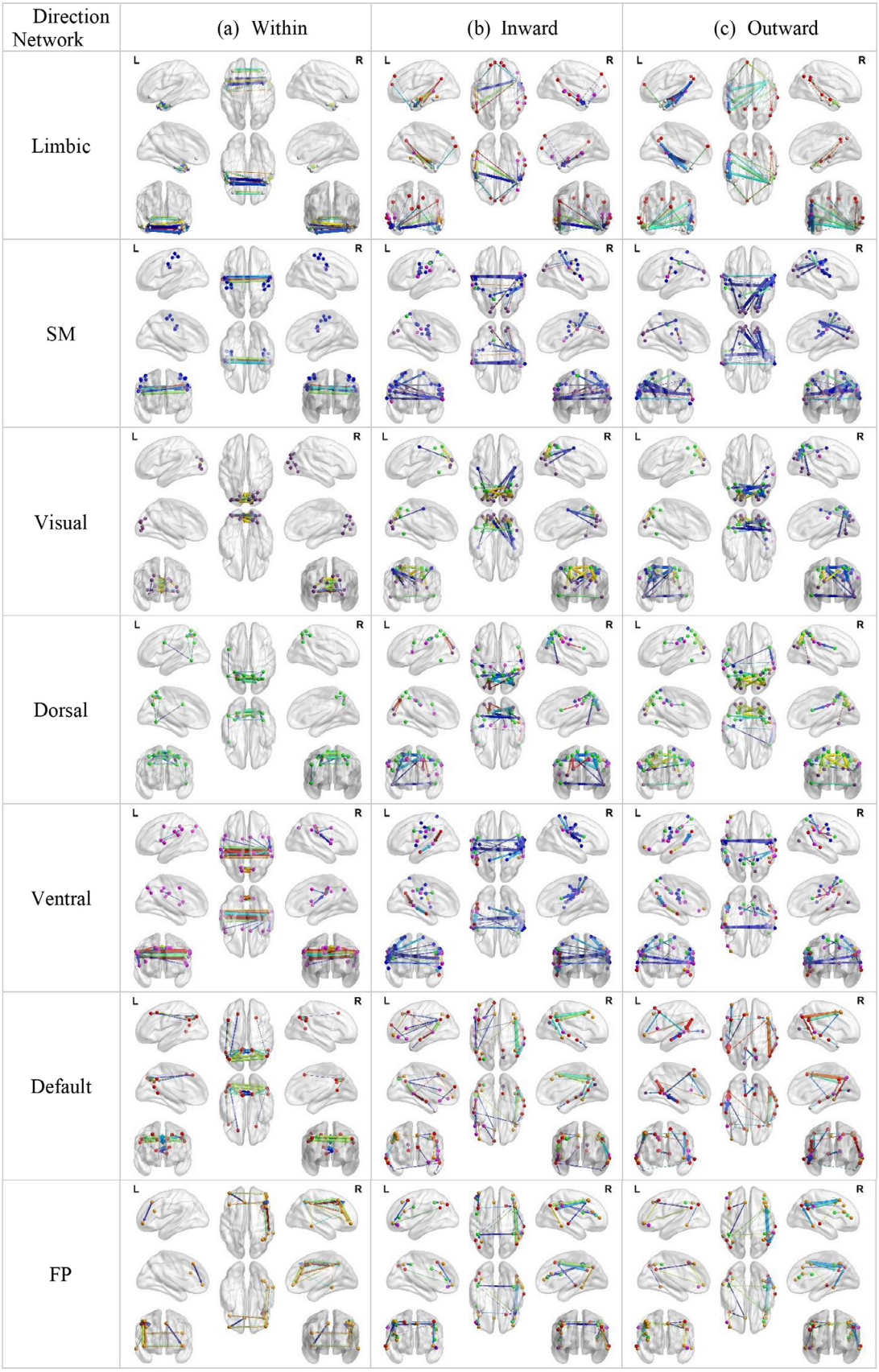

Fig. 4. Spatiotemporal functional interactivity in resting-state brain networks. The top 25 strongest connections within (a), coming into (b), and going out of (c) each of the seven functional brain networks is visualized by a modified version of BrainNet Viewer toolbox (Xia et al., 2013). The duration and the strength of the information are jointly displayed. In particular, the color of the arrow from cold to hot represents the duration from long to short. The thickness of the arrow represents the strength of the connectivity. So, stronger and longer connectivity has a thicker and warmer colored arrow. ROIs in each of the seven networks share the same network color as shown in the legend of Fig. 3 (right).

Table 1
The average duration (ms) of the inward and outward information transfer and their differences for each network.

Direction Network	Inward	Outward	Inward-Outward Differences
SM	1205 ± 345	1371 ± 517	-166 ± 643
Visual	1581 ± 527	1130 ± 370	451 ± 659
Dorsal	1355 ± 442	1186 ± 392	169 ± 565
Ventral	1198 ± 396	1313 ± 457	-115 ± 586
Default	1199 ± 389	1071 ± 301	127 ± 502
FP	1257 ± 296	1063 ± 295	195 ± 402
Limbic	862 ± 150	1218 ± 355	-355 ± 389

works are in Figure S9-S11 in the Supplementary Methods and Results. In addition, the top 1% strongest directed connections within, going out of, and coming into each of the seven functional brain networks are in Fig. S12. These figures clearly show that the inward-outward asymmetries are much more pronounced for the duration versus the strength estimates, and this pattern is observed for every network and even for every ROIs.

Statistically, each pair of ROIs has an average of inward-outward differences of -0.02 ± 0.25 (i.e., $\mu_{FC} = -0.02,\ std_{FC} = 0.25$) in the z-scores of directed RSFC strengths, and of -0.08 ± 1.38 (i.e., $\mu_D = -0.08,\ std_D = 1.38$) in the z-scores of durations. Then, z-test statistics is $Z_{FC0} = -19.755 < -Z_{\frac{\alpha}{2}}$ for the directed FC strength case, and it is $Z_{D0} = -13.765 < -Z_{\frac{\alpha}{2}}$ for the duration case. In other words, the two z-tests, one for the inward-outward differences in directed FC strength and the other for the inward-outward differences in duration, both reject the hypothesis of a zero-mean at a significance level of $\alpha = 5\%$. Moreover, the correlation between the upper and lower triangular entries of the z-score matrix of directed FC strength is as high as 0.9682. In contrast, this value becomes as low as 0.0464 for the duration z-score matrix. This indicates the duration of the pairwise connections having a higher degree of asymmetry comparing to the directed FC strength. This is further validated by the two-sample z-tests. Specifically, the two-sample z-test statistics $Z_0 = -9.9836 < -1.645 = -Z_\alpha$, which rejects the null hypothesis at a significance level of $\alpha = 5\%$. The p-value of this test $P(Z \le Z_0) = 1.7982 \times 10^{-23}$ is almost close to zero, which provides strong statistical evidence that the inward-outward differences in duration are greater than the inward-outward differences in FC strengths. The histograms of z-scores of all pairwise directed RSFC strengths and durations, as well as their inward-outward differences, are shown in Fig. S11.

We next evaluated the asymmetries in the duration matrices in more detail. Average durations for inward and outward information transfer for each network as well as their differences are presented in Table 1. Visual and Limbic networks show the greatest inward-outward differences in duration. In contrast, the Ventral and Default networks have more similar inward and outward connections in duration. The duration of information transfers for the SM, Ventral, and Limbic networks are generally shorter for inward versus outward connections, whereas all other networks show the reverse pattern, with shorter duration outward versus inward connections. Overall, the Limbic, Ventral, and Default networks have the shortest inward information transfers, whereas FP, Default, and Visual networks have the shortest outward information transfers.

Average durations of the inward and outward information transfers and their differences for each ROI are displayed in Fig. 5. Examining specific asymmetry patterns, the occipital lobe (Visual and Dorsal ROIs) displays the greatest temporal asymmetry with the longest inward and shortest outward durations. In contrast, the Limbic ROI shows the reverse pattern, with the shortest duration inward connection but the second-longest outward connection. The Ventral and SM ROIs show a somewhat more balanced duration pattern, albeit with overall longer outward than inward durations. ROIs within the PFC show the most equivalent inward and outward pattern, with nearly identical durations (~1300 ms). Finally, as observed in Fig 5, there are nodal differences in duration asymmetry within networks. For example, the Default network precuneus ROI shows a longer inward and shorter outward duration pattern, whereas the medial prefrontal ROIs of the default network shows shower inward and shorter outward duration patterns.

4. Discussion

Here we used a novel approach, p-correlation, to estimate the direction and duration of information transfer within a resting-state fMRI dataset. The p-correlation method decomposes the traditional pairwise functional interactivity into inward and outward functional connectivity. The connection strength, as well as the duration of the information transfer, are estimated for each direction. This method enables us to measure the direction (inward versus outward) and the duration (long versus short) connectivity profiles for all ROI-ROI pairs. The resulting whole-brain, directed functional connectivity and duration matrices revealed distinct network and regional patterns of spatiotemporal connectivity within the resting brain.

Note that the duration of information transfer from one region to another as is estimated in this paper is distinct from the time delay for a signal sent from one region to another. The 'duration of information transfer' in our definition refers to the length of time that the information is embedded within a communication channel (i.e., a functional connection). While the time delay for transferring one information unit between regions may be dependent on the physical distance between those regions, the 'duration of information transfer', which is represented as the input versus output delay, is not necessarily distance dependent.

Long vs. *short duration connections*. Long duration information transfers are observed within the somatomotor, visual, and dorsal attention networks. These long duration connections are highly overlapping with the stronger directed connections (Fig. 1). The shortest information transfers, on the other hand, are driven by multiple high-degree outward brain hubs in the visual and default systems (i.e., rows with dense dotted lines in Fig. 2) as well as several moderate high-degree inward brain hubs in the hippocampus (i.e., columns with less dense dotted lines in Fig. 2). The outward hubs, that segregate information from the visual or the default systems to the other cortical regions (as shown in Figs. 2(c) and 3(a)), in particular, are consistent with the previous findings of functional hubs in the cuneus of the visual system (Tomasi and Volkow, 2011) as well as the angular gyrus of default mode system (Andrews-Hanna et al., 2014). Our results further suggest that the role of these high-degree brain hubs is actively propagating the information to, instead of receiving the information from, other brain regions on a short temporal scale. In addition, the inward brain hubs in the limbic system which aggregate the information from the cortex (as shown in Figs. 2(c) and 3(b)), is consistent with the idea that resting-state brain function supports the memory consolidation (Gordon et al., 2014; Miall and Robertson, 2006; Stevens et al., 2010; Stevens and Spreng, 2014; Tambini et al., 2010). In our recent study, we have shown that the limbic regions, in particular, have greater contributions from high-frequency activity (Keilholz et al., 2020), which may play a role in determining the duration of information transfer**.** The inward and outward hubs were previously investigated on an average whole-brain level (Yan and He, 2011). Specifically, several functional hubs in the default network including the precuneus on average perform more like inward hubs than outward hubs as compared to other functional hubs. In contrast, functional hubs in the attentional network on average perform more like outward hubs. Our results extend these findings by suggesting specific contexts (e.g., at a short duration of information transfer) in which node-wise hubs may act differently from network averages.

Inward and outward asymmetry of the information transfer. In contrast to many other lag-based analytical approaches which assume the tem-

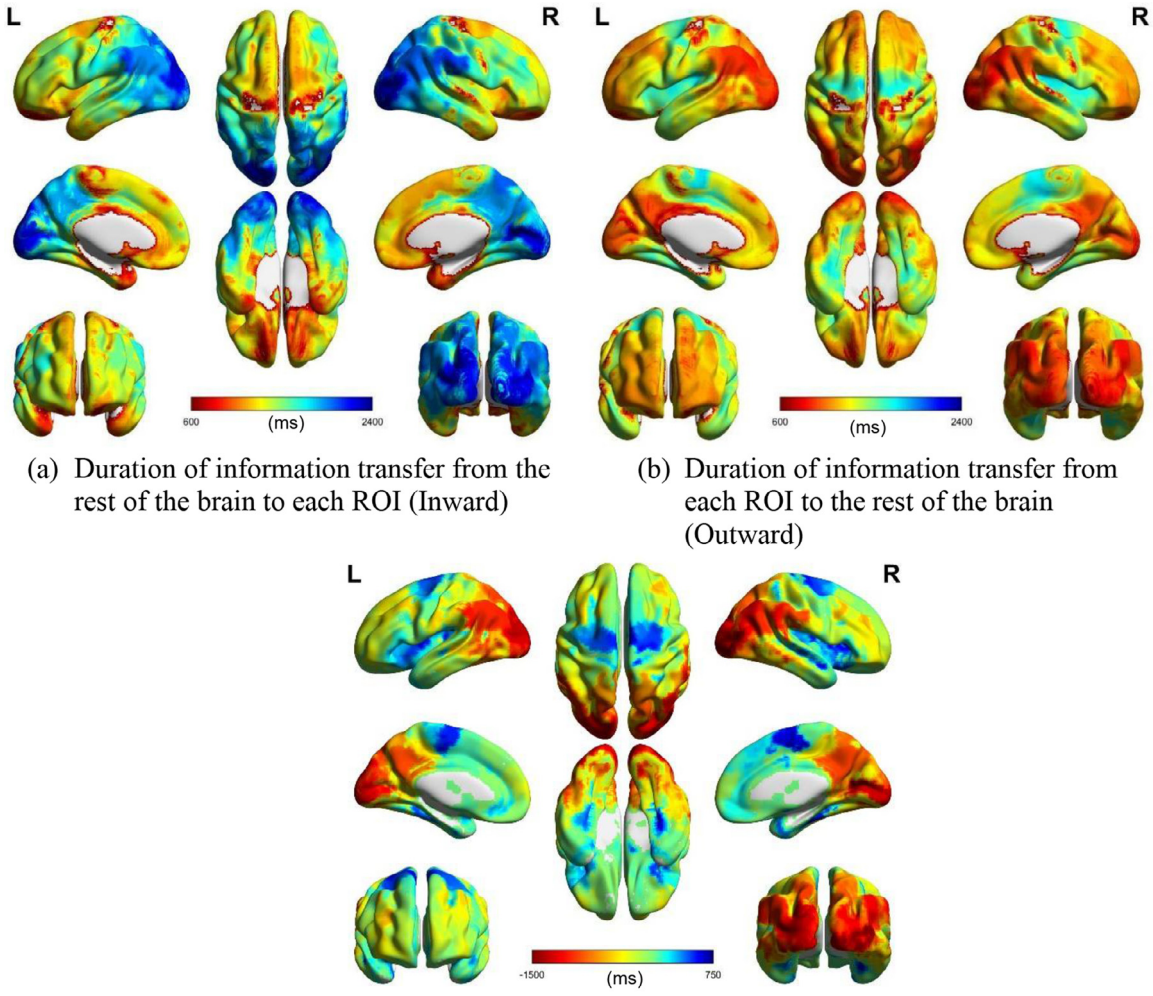

Fig. 5. The average duration (ms) of the information transfer coming from and going into each of the 333 ROIs provided in Gordon et al. (2016). For (a) and (b), the shortest information transfers have warm colors, while the longest information transfers have cool colors. Both inward and outward information transfers are displayed in the same colormap. For (c), the cool colors depict greater inward than the outward information transfers, while warm colors depict greater outward than the inward information transfers.

poral lags that are pairwise identical, e.g., (Mitra et al., 2015; Raut et al., 2020), we assume the functional interactivity can be pairwise asymmetric not only in the connection strength but also in the duration of the information transfer. In other words, ongoing information transfer in both forward and backward directions may simultaneously present in both spatial and temporal scales. Our findings, however, revealed only modest differences in the strength of directed pairwise connections (i.e. inward versus outward). Yet, there were striking asymmetries observed in the duration of these directed connections. This observation, as shown in Fig. 4, is persistent for every network and even for most ROI-ROI pairs. Previous studies have observed variability in lag-based temporal patterns (Bright et al., 2017; Raut et al., 2019; Smith et al., 2011), however, by splitting the study group, we have demonstrated that the asymmetries in duration are significant in comparison with asymmetries in strengths on an average level, and moreover, the duration of outward information transfer is significantly longer than the duration of the inward information transfer on average for each of the split groups. Furthermore, Fig. 4, which demonstrates the strongest directed connections within, going out of, and coming into each of the seven functional brain networks, provides a detailed description of the spatiotemporal functional interactivities on the brain cortex which may further our understanding of human cognition. In the end, the brain-wide duration of the information transfer was examined in more detail. As shown in Fig. 5, visual processing regions, including the precuneus, show longer duration of inward, or afferent, connections relative to shorter duration of outward, or efferent, connections. In contrast, regions of the limbic system show longer duration of outward, or efferent, connections relative to shorter duration of inward, or afferent connections. This is consistent with its role in consolidation processes, particularly involving medial temporal lobe regions (p. 313, Purves et al., 2008; Schwab et al., 2018). The prefrontal cortex on the other hand displayed inward and outward connections that were similar in duration, consistent with the role of this region as a heteromodal hub with dense, reciprocal connection to the rest of the cortex (Baars and Gage, 2013; Mesulam, 1998). Notably, the inward-outward differences in duration of information transfer as shown in Fig. 5(c) demonstrate close correspondence to the latency structure discovered in Fig. 1A (Raut et al., 2020). Specifically, in (Raut et al., 2020), by assuming the latency structure estimates are pairwise symmetric, the negative values/cool colors imply the inward latency in Fig. 1A (Raut et al., 2020). Comparatively, in the current work which assumed the pairwise connections to be asymmetric, the negative values/cool colors depict greater inward than the outward information transfers in Fig. 5(c). Similar temporal patterns appeared in the somatomotor, the precuneus, and the medial occipital cortex.

Strengths and limitations. Comparing to the existing methods for estimating the effective connectivity, p-correlation has many distinctions and merits. A group of effective connectivity estimation methods, which have been extensively used in neuroscience, are autoregressive based models, which include the transfer entropy (Timme and Lapish, 2018; Ursino et al., 2020), the Granger causality statistic (Seth et al., 2015), and other multivariate vector autoregressive models (MVAR) (Kuś et al., 2004; Ligeza et al., 2016; Wilke et al., 2008). Different from these methods, the causal model embedded in the p-correlation method (Eq. (1)) is a linear regression model but not autoregressive. More specifically, in contrast to the widely used Granger causality statistic, which assumes errors of the autoregressive model to be Gaussian, p-correlation is based only on the sample variance of the prediction error and does not require a Gaussian assumption on the noise. This is advantageous if the BOLD signals lack Gaussian structure. In practice, for transfer entropy, prior knowledge of the time lag is usually required before applying the algorithms (Liu and Zhang, 2019; Timme and Lapish, 2018), and for Granger causality, a common lag is required by the model for afferent and efferent connections (Smith et al., 2011) or for the connections among all ROIs (Seth, 2010; Smith et al., 2011; Stokes and Purdon, 2017). For p-correlation, however, a model order selection (Akaike, 1970; Cavanaugh, 1997; Schwarz, 1978) is integrated into the computation to estimate the lag length for each directed pair of signals. Moreover, the effective connectivity methods, such as transfer entropy, measure how much information is transferred from one signal to another, but are not a direct measure of causal coupling strength of signals (Ursino et al., 2020). In contrast, p-correlation, embedding a linear time-invariant causal system that delineates the information transfer (Eq. (1)), computes the strength of the directed functional connectivity for the static functional brain network, and indeed, p-correlation has performed well on both synthetic and experimental fMRI data (Xu et al., 2017).

Other than the autoregressive models, dynamic causal modeling (DCM) (Friston et al., 2003) has also been used to assess causal dynamics in fMRI data. As discussed in (p. 878, Smith et al., 2011), most existing DCM algorithms require knowledge of external inputs (which are not known for rs-fMRI) although some variations may not (Daunizeau et al., 2009). In contrast, p-correlation like correlation is a completely data-driven approach. In addition, while DCM has demonstrated success in estimating the effective connectivity for small networks with a small number of nodes, it has been a challenge for all versions of DCM scaling to networks with large numbers of ROIs which are necessary for experimental studies of whole human brains (Smith et al., 2011). In contrast, the p-correlation approach described in this paper scales similarly to a correlation approach for which hundreds of ROIs are not a challenge (Xu et al., 2014, 2017). Moreover, DCM imposes a common lag for all ROI interactions, whereas p-correlation estimates an asymmetric duration of information transfer between every ROI-ROI pairs, which provides in dynamics not only in the spatial but also in the temporal scale. Most importantly, a significant merit of p-correlation is that the estimated strength of directed functional connectivity (Eq. (3)) can be used to reliably detect the previously identified functional network organization of the human brain (Fig. 8, Xu et al., 2017), which has not been achieved by any autoregressive model (Stokes and Purdon, 2017) or DCM described above.

Despite these advantages, the calculation of duration of information transfer estimated by p-correlation is limited by the temporal sampling rate. As such, only spontaneous directed brain activities in the resting brain that are longer than 1 TR can be detected by the method. Note also that slice timing correction was not applied in the HCP data set, which could bias the calculation of short durations of information transfer. However, because the hemodynamic dynamic response function acts as a ~0.1 Hz low pass filter which greatly attenuates everything with a period shorter than ~10 s, the slice timing correction for a 1 TR (720 ms in our data) has a relatively small effect. Numerically, from Table 1 and Fig. 5, the average duration of information transfer for each network or each ROI ranges up to 3 TRs, whereas the inward-outward asymmetries could be within $\pm$1TR. As both temporal sampling and the lack of slice timing corrections could influence small differences in timing, the temporal information smaller or equal to 1 TR might result from the acquisition protocol which has no physiological significance. Hence, the inward-outward asymmetries might only reflect the relative value but not the accurate values in durations. Nevertheless, p-correlation is a measure that is adaptable to any type of timeseries, which enables us to explore the neural information processing in detail on the electrophysiological data such as EEG and MEG that have a finer timescale and higher SNR. In addition, while the present study is focused on the cerebral cortical organization, planned investigations will extend our study of spatiotemporal functional interactivities in subcortical and cerebellar structures.

Conclusions. As reviewed above, the p-correlation method provides novel insights into the spatiotemporal connectivity patterns in the resting brain. To our knowledge, this is the first method to concurrently estimate the strength, direction and duration of resting-state connectivity. As such, this method opens new avenues for understanding not only large-scale coherence patterns in the resting brain but also their temporal dynamics. This latter aspect, revealed by p-correlation, may serve as a proxy for investigating the nature of information flow through the intrinsic functional architecture of the brain. These insights in turn open a novel frontier for investigating associations between the intrinsic functional connectivity of the brain and human behavior.

Credit author statement

Nan Xu: Conceptualization, Methodology, Formal analysis, Visualization, Writing - original draft, Writing - review & editing.

Peter C. Doerschuk: Writing - review & editing

Shella D. Keilholz: Methodology, Writing - review & editing.

R. Nathan Spreng: Conceptualization, Methodology, Writing-review & editing

Shella D. Keilholz and **R. Nathan Spreng** have equal contributions.

Data availability

The data that support the findings of this study are openly available in Human Connectome Project 500 Subjects + MEG2 dataset (https://www.humanconnectome.org/study/hcp-young-adult/document/500-subjects-data-release) at Van Essen, Smith et al. (2013).

Van Essen, D. C., S. M. Smith, D. M. Barch, T. E. Behrens, E. Yacoub, K. Ugurbil and W. U.-M. H. Consortium (2013). "The WU-Minn Human Connectome Project: an overview." Neuroimage **80**: 62–79.

Acknowledgment

"Data were provided [in part] by the Human Connectome Project, WU-Minn Consortium (Principal Investigators: David Van Essen and Kamil Ugurbil; 1U54MH091657) funded by the 16 NIH Institutes and Centers that support the NIH Blueprint for Neuroscience Research; and by the McDonnell Center for Systems Neuroscience at Washington University." NX and SDK thank National Science Foundation (grant 1533260) for funding support. PCD thanks National Science Foundation (grant 1217867) for funding support. RNS thanks the support by the Natural Sciences and Engineering Research Council of Canada and Canadian Institutes of Health Research, and the Research Scholar support by Fonds de recherche du Québec – Santé. The authors thank Dr. Xie Yao Chen from Georgia Institute of Technology H. Milton Stewart School of Industrial & Systems Engineering for the helpful discussion of setting up hypothesis testing on inward-outward asymmetries.

Supplementary materials

Supplementary material associated with this article can be found, in the online version, at doi:10.1016/j.neuroimage.2020.117628.

References

Akaike, H., 1970. Statistical predictor identification. Ann. Inst. Stat. Math. 22 (1), 203–217. doi:10.1007/BF02506337.

Andrews-Hanna, J.R., Smallwood, J., Spreng, R.N., 2014. The default network and self-generated thought: component processes, dynamic control, and clinical relevance. Ann. N. Y. Acad. Sci. 1316 (1), 29–52. doi:10.1111/nyas.12360.

Baars, B., Gage, N., 2013. Fundamentals of cognitive neuroscience : a beginner's guide. In: Gage, N.M. (Ed.), Fundamentals of Cognitive Neuroscience. Elsevier Science. doi:10.1016/c2014-0-03767-7.

Biswal, B.B., Mennes, M., Zuo, X.N., Gohel, S., Kelly, C., Smith, S.M., Beckmann, C.F., Adelstein, J.S., Buckner, R.L., Colcombe, S., Dogonowski, A.M., et al., 2010. Toward discovery science of human brain function. Proc. Natl. Acad. Sci. U.S.A. 107 (10), 4734–4739. doi:10.1073/pnas.0911855107.

Biswal, B., Yetkin, F.Z., Haughton, V.M., Hyde, J.S., 1995. Functional connectivity in the motor cortex of resting human brain using echo-planar MRI. Magn. Reson. Med. 34 (4), 537–541. https://www.ncbi.nlm.nih.gov/pubmed/8524021.

Blinowska, K.J., Trzaskowski, B., Kaminski, M., Kus, R., 2009. Multivariate autoregressive model for a study of phylogenetic diversity. Gene 435 (1–2), 104–118. doi:10.1016/j.gene.2009.01.009.

Bright, M.G., Tench, C.R., Murphy, K., 2017. Potential pitfalls when denoising resting state fMRI data using nuisance regression. Neuroimage 154, 159–168. doi:10.1016/j.neuroimage.2016.12.027.

Buckner, R.L., Sepulcre, J., Talukdar, T., Krienen, F.M., Liu, H., Hedden, T., Andrews-Hanna, J.R., Sperling, R.A., Johnson, K.A., 2009. Cortical hubs revealed by intrinsic functional connectivity: mapping, assessment of stability, and relation to Alzheimer's disease. J. Neurosci. 29 (6), 1860–1873. doi:10.1523/JNEUROSCI.5062-08.2009.

Cavanaugh, J.E., 1997. Unifying the derivations for the Akaike and corrected Akaike information criteria. Stat. Probab. Lett. 33 (2), 201–208. doi:10.1016/s0167-7152(96)00128-9.

Chen, G., Glen, D.R., Saad, Z.S., Paul Hamilton, J., Thomason, M.E., Gotlib, I.H., Cox, R.W., 2011. Vector autoregression, structural equation modeling, and their synthesis in neuroimaging data analysis. Comput. Biol. Med. 41 (12), 1142–1155. doi:10.1016/j.compbiomed.2011.09.004.

Cole, M.W., Bassett, D.S., Power, J.D., Braver, T.S., Petersen, S.E., 2014. Intrinsic and task-evoked network architectures of the human brain. Neuron 83 (1), 238–251. doi:10.1016/j.neuron.2014.05.014.

Daunizeau, J., Friston, K.J., Kiebel, S.J., 2009. Variational Bayesian identification and prediction of stochastic nonlinear dynamic causal models. Phys. D 238 (21), 2089–2118. doi:10.1016/j.physd.2009.08.002.

Friston, K.J., Harrison, L., Penny, W., 2003. Dynamic causal modelling. Neuroimage 19 (4), 1273–1302. doi:10.1016/S1053-8119(03)00202-7.

Glasser, M.F., Sotiropoulos, S.N., Wilson, J.A., Coalson, T.S., Fischl, B., Andersson, J.L., Xu, J., Jbabdi, S., Webster, M., Polimeni, J.R., Van Essen, D.C., Jenkinson, M.WU-Minn HCP Consortium, 2013. The minimal preprocessing pipelines for the human connectome project. Neuroimage 80, 105–124. doi:10.1016/j.neuroimage.2013.04.127.

Goelman, G., Dan, R., Ruzicka, F., Bezdicek, O., Ruzicka, E., Roth, J., Vymazal, J., Jech, R., 2017. Frequency-phase analysis of resting-state functional MRI. Sci. Rep. 7, 43743. doi:10.1038/srep43743.

Gordon, E.M., Breeden, A.L., Bean, S.E., Vaidya, C.J., 2014. Working memory-related changes in functional connectivity persist beyond task disengagement. Hum. Brain Mapp. 35 (3), 1004–1017. doi:10.1002/hbm.22230.

Gordon, E.M., Laumann, T.O., Adeyemo, B., Huckins, J.F., Kelley, W.M., Petersen, S.E., 2016. Generation and evaluation of a cortical area parcellation from resting-state correlations. Cereb. Cortex 26 (1), 288–303. doi:10.1093/cercor/bhu239.

Griffanti, L., Salimi-Khorshidi, G., Beckmann, C.F., Auerbach, E.J., Douaud, G., Sexton, C.E., Zsoldos, E., Ebmeier, K.P., Filippini, N., Mackay, C.E., Moeller, S., Xu, J., Yacoub, E., Baselli, G., Ugurbil, K., Miller, K.L., Smith, S.M., 2014. ICA-based artefact removal and accelerated fMRI acquisition for improved resting state network imaging. Neuroimage 95, 232–247. doi:10.1016/j.neuroimage.2014.03.034.

Keilholz, S.D., Maltbie, E.A., Zhang, X., Yousefi, B., Pan, W.J., Xu, N., Nezafati, M., LaGrow, T.J., Guo, Y., 2020. Relationship between basic properties of BOLD fluctuations and calculated metrics of complexity in the human connectome project. Front. Neurosci. doi:10.3389/fnins.2020.550923.

Kim, J., Zhu, W., Chang, L., Bentler, P.M., Ernst, T., 2007. Unified structural equation modeling approach for the analysis of multisubject, multivariate functional MRI data. Hum. Brain Mapp. 28 (2), 85–93. doi:10.1002/hbm.20259.

Kuś, R., Kamiński, M., Blinowska, K.J., 2004. Determination of EEG activity propagation: pair-wise versus multichannel estimate. IEEE Trans. Biomed. Eng. 51 (9), 1501–1510. doi:10.1109/TBME.2004.827929.

Ligeza, T.S., Wyczesany, M., Tymorek, A.D., Kamiński, M., 2016. Interactions between the prefrontal cortex and attentional systems during volitional affective regulation: an effective connectivity reappraisal study. Brain Topogr. 29 (2), 253–261. doi:10.1007/s10548-015-0454-2.

Liu, Y., Zhang, N., 2019. Propagations of spontaneous brain activity in awake rats. Neuroimage 202, 116176. doi:10.1016/j.neuroimage.2019.116176.

Marcus, D.S., Harwell, J., Olsen, T., Hodge, M., Glasser, M.F., Prior, F., Jenkinson, M., Laumann, T., Curtiss, S.W., Van Essen, D.C., 2011. Informatics and data mining tools and strategies for the human connectome project. Front. Neuroinform. 5, 4. doi:10.3389/fninf.2011.00004.

Mesulam, M.M., 1998. From sensation to cognition. Brain 121, 1013–1052. doi:10.1093/brain/121.6.1013, *(Pt 6*.

Miall, R.C., Robertson, E.M., 2006. Functional imaging: is the resting brain resting? Curr. Biol. 16 (23), R998–1000. doi:10.1016/j.cub.2006.10.041.

Mitra, A., Snyder, A.Z., Blazey, T., Raichle, M.E., 2015. Lag threads organize the brain's intrinsic activity. Proc. Natl. Acad. Sci. U. S. A. 112 (17), E2235–E2244. doi:10.1073/pnas.1503960112.

Montgomery, D.C., Runger, G.C., 2010. Applied Statistics and Probability For Engineers. John Wiley & Sons.

Murphy, K., Fox, M.D., 2017. Towards a consensus regarding global signal regression for resting state functional connectivity MRI. Neuroimage 154, 169–173. doi:10.1016/j.neuroimage.2016.11.052.

Power, J.D., Cohen, A.L., Nelson, S.M., Wig, G.S., Barnes, K.A., Church, J.A., Vogel, A.C., Laumann, T.O., Miezin, F.M., Schlaggar, B.L., Petersen, S.E., 2011. Functional network organization of the human brain. Neuron 72 (4), 665–678. doi:10.1016/j.neuron.2011.09.006.

Power, J.D., Schlaggar, B.L., Lessov-Schlaggar, C.N., Petersen, S.E., 2013. Evidence for hubs in human functional brain networks. Neuron 79 (4), 798–813. doi:10.1016/j.neuron.2013.07.035.

Press, W.H., Teukolsky, S.A., Vetterling, W.T., Flannery, B.P., 2007. Numerical Recipes: The Art of Scientific Computing. Cambridge University Press https://www.amazon.com/Numerical-Recipes-3rd-Scientific-Computing/dp/0521880688.

Purves, D., Cabeza, R., Huettel, S.A., LaBar, K.S., Platt, M.L., Woldorff, M.G.Duke University. Center for Cognitive Neuroscience, 2008. Principles of Cognitive Neuroscience. Sinauer Associates.

Raut, Ryan V., Mitra, A., Snyder, A.Z., Raichle, M.E., 2019. On time delay estimation and sampling error in resting-state fMRI. Neuroimage 194, 211–227. doi:10.1016/j.neuroimage.2019.03.020.

Raut, R.V., Mitra, A., Marek, S., Ortega, M., Snyder, A.Z., Tanenbaum, A., Laumann, T.O., Dosenbach, N.U.F., Raichle, M.E., 2020. Organization of propagated intrinsic brain activity in individual humans. Cereb. Cortex 30 (3), 1716–1734. doi:10.1093/cercor/bhz198.

Roebroeck, A., Formisano, E., Goebel, R., 2005. Mapping directed influence over the brain using Granger causality and fMRI. Neuroimage 25 (1), 230–242. doi:10.1016/j.neuroimage.2004.11.017.

Salimi-Khorshidi, G., Douaud, G., Beckmann, C.F., Glasser, M.F., Griffanti, L., Smith, S.M., 2014. Automatic denoising of functional MRI data: combining independent component analysis and hierarchical fusion of classifiers. Neuroimage 90, 449–468. doi:10.1016/j.neuroimage.2013.11.046.

Schwab, S., Harbord, R., Zerbi, V., Elliott, L., Afyouni, S., Smith, J.Q., Woolrich, M.W., Smith, S.M., Nichols, T.E., 2018. Directed functional connectivity using dynamic graphical models. Neuroimage 175, 340–353. doi:10.1016/j.neuroimage.2018.03.074.

Schwarz, G., 1978. Estimating the dimension of a model. Ann. Stat. 6 (2), 461–464. doi:10.1214/aos/1176344136.

Seth, A.K., 2010. A MATLAB toolbox for Granger causal connectivity analysis. J. Neurosci. Methods 186 (2), 262–273. doi:10.1016/j.jneumeth.2009.11.020.

Seth, A.K., Barrett, A.B., Barnett, L., 2015. Granger causality analysis in neuroscience and neuroimaging. J. Neurosci. 35 (8), 3293–3297. doi:10.1523/JNEUROSCI.4399-14.2015.

Smith, S.M., Miller, K.L., Salimi-Khorshidi, G., Webster, M., Beckmann, C.F., Nichols, T.E., Ramsey, J.D., Woolrich, M.W., 2011. Network modelling methods for FMRI. Neuroimage 54 (2), 875–891. doi:10.1016/j.neuroimage.2010.08.063.

Sporns, O., 2011. The human connectome: a complex network. Ann. N. Y. Acad. Sci. 1224, 109–125. doi:10.1111/j.1749-6632.2010.05888.x.

Stevens, W.D., Buckner, R.L., Schacter, D.L., 2010. Correlated low-frequency BOLD fluctuations in the resting human brain are modulated by recent experience in category-preferential visual regions. Cereb. Cortex 20 (8), 1997–2006. doi:10.1093/cercor/bhp270.

Stevens, W.D., Spreng, R.N., 2014. Resting-state functional connectivity MRI reveals active processes central to cognition. Wiley Interdiscip. Rev. Cognit. Sci. 5 (2), 233–245. doi:10.1002/wcs.1275.

Stokes, P.A., Purdon, P.L., 2017. A study of problems encountered in Granger causality analysis from a neuroscience perspective. Proc. Natl. Acad. Sci. U.S.A. 114 (34), E7063–E7072. doi:10.1073/pnas.1704663114.

Tambini, A., Ketz, N., Davachi, L., 2010. Enhanced brain correlations during rest are related to memory for recent experiences. Neuron 65 (2), 280–290. doi:10.1016/j.neuron.2010.01.001.

Timme, N.M., Lapish, C., 2018. A tutorial for information theory in neuroscience. Eneuro. Society for Neuroscience (Vol. 5, Issue 3) doi:10.1523/ENEURO.0052-18.2018.

Tomasi, D., Volkow, N.D., 2011. Association between functional connectivity hubs and brain networks. Cereb. Cortex 21 (9), 2003–2013. doi:10.1093/cercor/bhq268.

Ursino, M., Ricci, G., Magosso, E., 2020. Transfer entropy as a measure of brain connectivity: a critical analysis with the help of neural mass models. Front. Comput. Neurosci. 14, 45. doi:10.3389/fncom.2020.00045.

Van Essen, D.C., Ugurbil, K., Auerbach, E., Barch, D., Behrens, T.E., Bucholz, R., Chang, A., Chen, L., Corbetta, M., Curtiss, S.W., Della Penna, S., Feinberg, D., Glasser, M.F., Harel, N., Heath, A.C., Larson-Prior, L., Marcus, D., Michalareas, G., … Moeller, S.Consortium, W. U.-M. H. C. P., 2012. The human connectome project: a data acquisition perspective. Neuroimage 62 (4), 2222–2231. doi:10.1016/j.neuroimage.2012.02.018.

Wig, G.S., Schlaggar, B.L., Petersen, S.E., 2011. Concepts and principles in the analysis of brain networks. Ann. N. Y. Acad. Sci. 1224, 126–146. doi:10.1111/j.1749-6632.2010.05947.x.

Wilke, C., Ding, L., He, B., 2008. Estimation of time-varying connectivity patterns through the use of an adaptive directed transfer function. IEEE Trans. Biomed. Eng. 55 (11), 2557–2564. doi:10.1109/TBME.2008.919885.

Xia, M., Wang, J., He, Y., 2013. BrainNet Viewer: a network visualization tool for human brain connectomics. PLoS One 8 (7), e68910. doi:10.1371/journal.pone.0068910.

Xu, N., Spreng, R.N., Doerschuk, P.C., 2014. Directed interactivity of large-scale brain networks: introducing a new method for estimating resting-state effective connectivity MRI. In: Proceedings of the IEEE International Conference on Image Processing, ICIP 2014 doi:10.1109/ICIP.2014.7025712.

Xu, N., Spreng, R.N., Doerschuk, P.C., 2017. Initial validation for the estimation of resting-state fMRI effective connectivity by a generalization of the correlation approach. Front. Neurosci. (MAY) 11. doi:10.3389/fnins.2017.00271.

Yan, C., He, Y., 2011. Driving and driven architectures of directed small-world human brain functional networks. PLoS One 6 (8), e23460. doi:10.1371/journal.pone.0023460.

Yeo, B.T., Krienen, F.M., Sepulcre, J., Sabuncu, M.R., Lashkari, D., Hollinshead, M., Roffman, J.L., Smoller, J.W., Zollei, L., Polimeni, J.R., Fischl, B., Liu, H., Buckner, R.L., 2011. The organization of the human cerebral cortex estimated by intrinsic functional connectivity. J. Neurophysiol. 106 (3), 1125–1165. doi:10.1152/jn.00338.2011.

Yuste, R., Fairhall, A.L., 2015. Temporal dynamics in fMRI resting-state activity. Proc. Natl. Acad. Sci. U. S. A. 112 (17), 5263–5264. doi:10.1073/pnas.1505898112.